INL/CON-08-14892
PREPRINT

Experimental Investigation of Material Flows Within FSWs Using 3D Tomography

Trends in Welding Research, 8th International Conference

Charles R. Tolle
Timothy A. White
Karen S. Miller
Denis E. Clark
Herschel B. Smartt

June 2008

The INL is a
U.S. Department of Energy
National Laboratory
operated by
Battelle Energy Alliance

Experimental Investigation of Material Flows Within FSWs Using 3D Tomography

Charles R. Tolle*, Timothy A. White, Karen S. Miller, Denis E. Clark, and Herschel B. Smartt
Idaho National Laboratory, Energy Efficiency and Industrial Technologies, Idaho Falls, Idaho, USA
**Charles.Tolle@inl.gov, 208-526-1895, fax 208-526-0690*

Abstract

There exists significant prior work using tracers or pre-placed hardened markers within friction stir welding (FSWing) to experimentally explore material flow within the FSW process. Our experiments replaced markers with a thin sheet of copper foil placed between the 6061 aluminum lap and butt joints that were then welded. The absorption characteristics of x-rays for copper and aluminum are significantly different allowing for non-destructive evaluation (NDE) methods such as x-ray computed tomography (CT) to be used to demonstrate the material movement within the weldment on a much larger scale than previously shown. 3D CT reconstruction of the copper components of the weldment allows for a unique view into the final turbulent state of the welding process as process parameters are varied. The x-ray CT data of a section of the weld region was collected using a cone-beam x-ray imaging system developed at the INL. Six-hundred projections were collected over 360-degrees using a 160-kVp Bremsstrahlung x-ray generator (25-micrometer focal spot) and amorphous-silicon x-ray detector. The region of the object that was imaged was about 3cm tall and 1.5cm x 1cm in cross section, and was imaged at a magnification of about 3.6x. The data were reconstructed on a 0.5x0.5x0.5 mm^3 voxel grid. After reconstruction, the aluminum and copper could be easily discriminated using a gray level threshold allowing visualization of the copper components. Fractal analysis of the tomographic reconstructed material topology is investigated as a means to quantify macro level material flow based on process parameters. The results of multi-pass FSWs show increased refinement of the copper trace material. Implications of these techniques for quantifying process flow are discussed.

Introduction

The objective of this paper is to explore the potential use of x-ray computed tomography (CT) and fractal analysis to further investigate material properties of friction stir welds produced using a variety of welding tools and methods. Since this is a feasibility study rather than an extensive parametric study of tooling, processes, and methods, we have used a simple sandwich-lap joint in which a tracer sheet of copper within an aluminum matrix serves as a marker to study mixing within lap and butt joints.

In this paper, we will only present a series of reconstructions for a particular lap weld. The 3D x-ray CT reconstruction of the broken up and redistributed copper within the weldment gives a useful view of the final turbulent state of the welding process. The intent is to compare the final state of a weld made with a particular set or parameters to other welds made with different process parameters to increase the general understanding of the relationship of process parameters to weldment properties.

In addition to a better understanding of weldment material properties, the overall uniformity and stability of the FSW process within weldments can be investigated by comparing the properties of segments along the weld's length. This requires a quantitative means of measuring the changes in the size and spatial distribution of entrained tracer particles. Furthermore, this requires quantifying structural characteristics across numerous length scales; which is an analysis problem shared across many technical fields, such as the development of new materials [1], and the analysis of medical, homeland security, Department of Defense, and DOE imagery [2–7]. Each of these applications requires a similar mathematical analysis to obtaining basic knowledge and quantify the underlying, fundamental properties of the spatially oriented sub-structures across the varying length scales.

Such a highly accurate spatially oriented structural model can be obtained via a generalized form of unified fractal statistics quantification techniques currently under development [8–10]. The first of these statistics, i.e., fractal dimension [11], has been well studied; however the remaining two, lacunarity and connectivity [5,8–13], have rarely been discussed in the open literature. It has been shown that by fusing fractal dimension and a term Musgrave refers to as a *lacunarity parameter* [14] (which we note as a combination of our lacunarity and connectivity), and using a chaos-like generation algorithm,

one can produce life-like terrain for digital imagery, similar to those seen in the movie industry with the production of life-like terrain for digital imagery.

Properly formulated, fractal statistics lend themselves to multi-dimensional data space analysis and quantification because they measure fundamental n-dimensional topological parameters. Thus, the new unified fractal statistics will be used to quantify the distribution of the copper tracer material within the prototypical CT-reconstructed friction stir welded examples shown within this paper. The results presented also show how multi-pass FSW (also known as friction stir processing (FSP)) can, as might be expected, further refine the average particle size of tracer materials with each processing pass (see Figure 4).

The prototypical Friction Stir weldments to be examined via the CT process will be briefly described, followed by a brief introduction to the x-ray CT process, with a sample reconstruction. Then fractal statistics will be visually correlated with the reconstructed FSW welds under investigation.

Experimental Setup

Materials

All FSWs were performed on 6061-T6511 aluminum base material. Coupon dimensions were nominally 4 in. x 8 in x 0.508 in., see the sandwich configuration in Figure 1. The sandwich material was clamped with 6 hold-downs, taken in pairs, nominally equal distance along the coupon, compressed against a steel tie down fixture approximately 2 in. thick, which can be water cooled (for these welds, the water cooling was turned off), as seen in Figure 2. Similar experiments have also been performed with the coupon affixed to a copper, water-cooled plate, nominally 24 in. x 5 in. Numerous sample plates have been created; although, due to the shortness of the project length and funding only one sample plate section has undergone tomographic reconstruction**.**

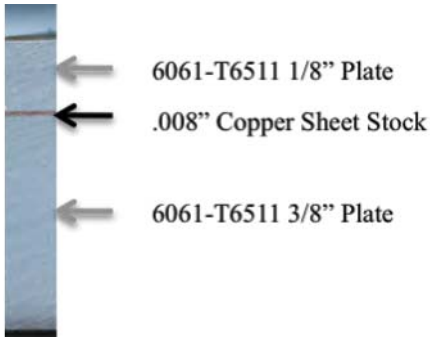

Figure 1: The experimental test sample consisted of a sandwich of 1/8" 6061-T6511 aluminum plate, 0.008 in. copper shim stock (SHOPAID Shim IN A CAN, Shop-Aid Inc. Woburn, MA 01801), and a 3/8" 6061-T6511 Aluminum plate. The FSW tool was normal to the top surface of the sandwich (i.e. the tool was oriented vertically downward in the image shown above).

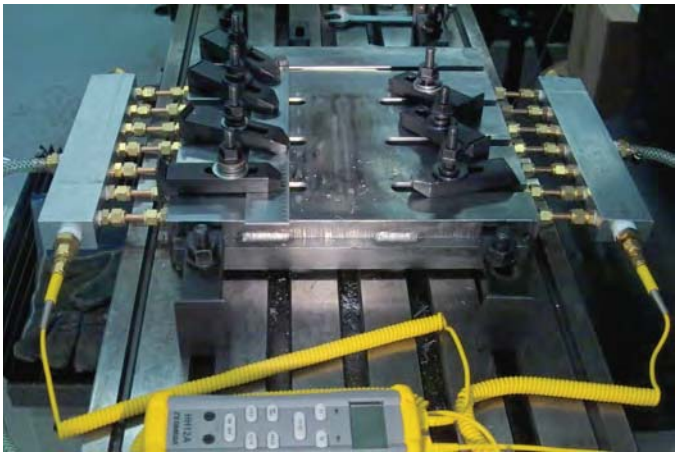

Figure 2: Experimental fixture. The fixture allows for the measurement of input and output cooling fluid temperatures which can be used to determine heat extraction amounts (not used within this set of experiments).

FSW Tools

The basic tool design is shown in Figure 3. The FSW tool was fashioned out of T15 tool steel. Little to no appreciable tool wear has been shown to occur, verified via visual inspection and scanning electron microscope (SEM) analysis of the welded region, see Figure 4.

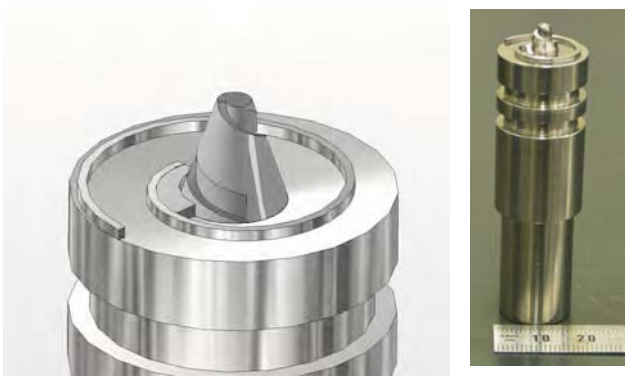

Figure 3: All tools were based on this scrolled pin and shoulder design. The witness ruler within the image on the right is in units of millimeters.

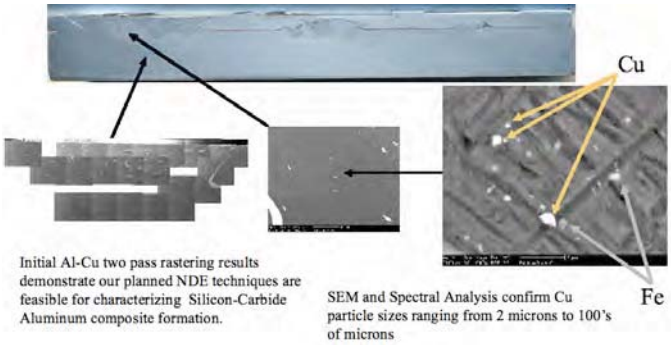

Figure 4: Scanning electron microscope (SEM) analysis of a small region within the tomographic reconstructed weld zone. This analysis shows that the copper particles entrained within the welded region range from hundreds of microns, down to only a few microns. Furthermore, minimal wear from the FSW tool is shown in that very few micron sized iron particles have become entrained within the weldment. Note that the copper particles in the bottom left image are smaller on the left side – i.e. the side that was processed twice.

FSW Procedures

Numerous welds were made with various travel speeds (from 4 inches per minute to 12 inches per minute) and rotational speeds (from 600 rpm to 2400 rpm). The tomographic reconstructions of prototypical FSWs presented here used a travel speed of 8 in./min and a tool rotational speeds of 1000, 1304, and 1304 rpm, as seen in Figure 4, reading left to right. The two left welds, within Figure 4, were also rastered, i.e., these welds were made in two passes. The second pass was adjacent to the first, so that the weld zones merged into one region while maintaining minimal overlap within the pin regions of each weld zone. The rotational tool speed remained constant for both the plunge and travel portions of the welds.

X-ray Computed Tomography

X-ray computed tomography (CT) is a technique for non-destructive evaluation (NDE) that shares the physics and mathematical background with its more commonly known imaging modality, the medical CAT scanner [15]. In recent years, CT has become a common tool in materials-characterization laboratories [16]. X-ray radiographs are two-dimensional (2D) projections of a three-dimensional (3D) object. By collecting radiographs from a set of viewing locations, for instance by collecting images as the object rotates, a 3D data set (2 dimensions in the radiograph and the rotation angle) is obtained, and these data are transformed into a 3D map of the material distribution in the object, see Figure 5. Using Bremstrahlung x-ray sources and conventional detectors, the pixel intensity in this 3D map is proportional to the density and effective atomic number of the object, essentially a map of the anatomy of the object. Because copper is substantially denser than aluminum, high contrast is achieved by using copper as the marker material in aluminum weldments.

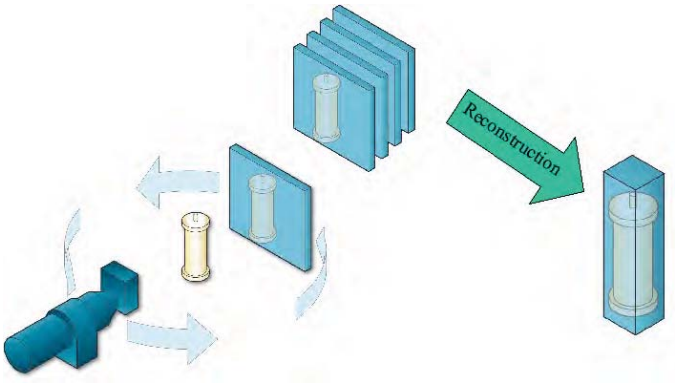

Figure 5: Schematic visualization of the X-ray Transmission Computed Tomography imaging process: Two dimensional x-ray images are projections of the material density and thickness in the object under examination. A set of projections is collected as the object is rotated through 360˚. These projections are processed in a reconstruction step to create a three-dimensional representation of the object in which the intensity of a volume element (voxel) is proportional to the material density in that region of the object. The density and atomic number of aluminum and copper are sufficiently different to be able to readily differentiate these materials in the data and determine copper distribution in the weld region.

In these experiments, we used a 3D cone-beam CT imaging system that has been developed at the Idaho National Laboratory. The system consists of a micro-focus x-ray tube, a 25cm by 20cm amorphous-silicon x-ray detector, a motion system for object manipulation, and an integrated computer-control system. Projection data were collected at 160kVp using a 25μm focal spot and a magnification (determined by optical geometry) of 3.6. Six hundred projections were collected as the weld sample was rotated through 360 degrees. Two example projections separated in angle by 90-degrees are shown in Figure 6. When these data are shown in sequence (e.g., as a movie), the distribution of copper material, including features such as swirls due to the tool motion, can easily be processed by the human eye and qualitatively visualized. However, it is difficult to perform any metrology because of the ambiguity in depth inherent in the projection process. The data were reconstructed using the cone-beam reconstruction algorithm developed by Feldkamp, Davis, and Kress [17]. Two slices from the 3D data set, one parallel and one perpendicular to the rotation axis, are shown in Figure 7. In the projection data (Figure 6), the pixel intensity is proportional to the line integral of the object density along a line from source to detector, however the reconstructed image is a map in which the pixel intensity is proportional to object density. From the reconstructed CT data it is possible to determine the distribution of copper in the weld zone. The actual x-ray CT system used is shown in Figure 8. By thresholding the images in Figure 7, a 3D data set of only the copper trace material can be visualized as in Figure 9. This is the type of data set to which we will apply fractal analysis.

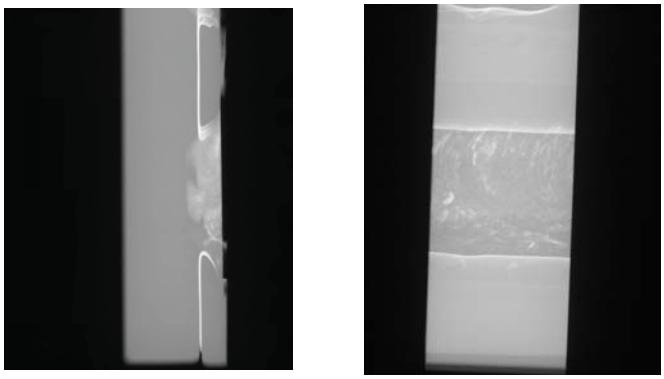

Figure 6: Side and top view projections of the weld sample looking into the lap weld joint. . The brighter/whiter areas contain copper, which has been either placed between the aluminum plates before the weld (Figure 1) or entrained into the weld joint during the FSW process (Figure 4). The pixel intensity shown in these images is proportional to the density and x-ray path length through the object, thereby making the copper regions brighter than the aluminum regions, i.e. this is best shown by the long paths through the copper sheet which result in the brightest portion of the left image.

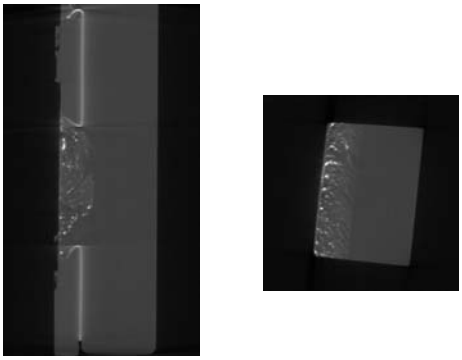

Figure 7: Sample CT slices from data in Figure X1. In the reconstructed images, the pixel intensity is proportional to the average density in a voxel. From this 3D data, accurate metrology and copper size and distribution can be determined.

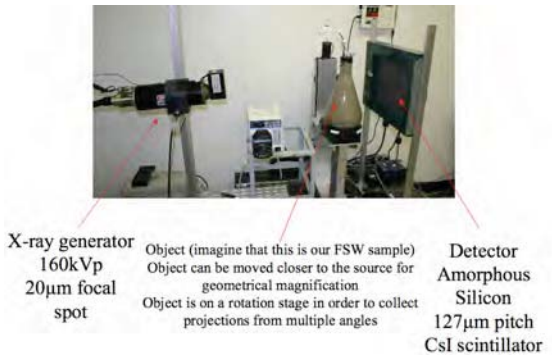

Figure 8: INL's developmental X-ray Transmission Computed Tomography (XTCT) imaging system. This system is used to analyze numerous types of targets, in this case a chemical compound is under analysis within the flask.

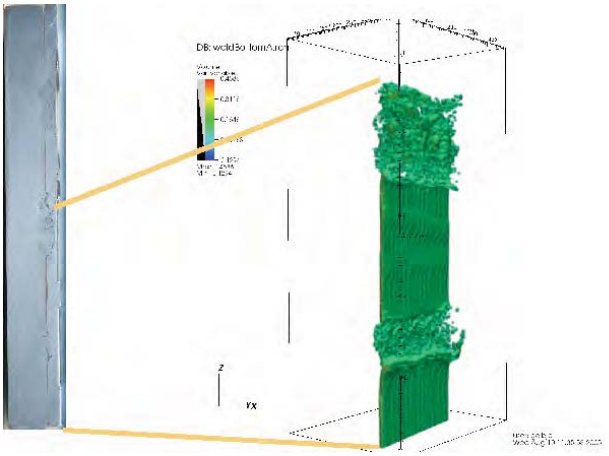

Figure 9: X-ray tomographic reconstruction thresheld pixel intensity to select only copper material, i.e. a "black and white" threshold limit was set so that the aluminum matrix disappeared leaving only the copper particles from within the weld region. Figures 6 and 7 are from the top weld shown above, while this thresheld reconstruction shown above is based on the bottom two welds.

Unified Fractal Analysis

Mandelbrot theorized that three parameters fully described a fractal's characteristics: fractal dimension, lacunarity, and what will be referred to here as connectivity [11]. Lacunarity and connectivity are largely unstudied, partly because these parameters lacked widely accepted rigorous definitions. One example of the effects of Musgrave's lacunarity [14] on image texture for a constant fractal dimension of 2.5 is shown in Figure 10 [14]. The importance of these fractal textures is that they demonstrate the effects of maintaining a constant fractal dimension while allowing the textural "look" to change significantly with a change in lacunarity and connectivity. Unfortunately, these texture generation algorithms are not general for n-dimensional data sets and Musgrave's lacunarity parameter is not based on any generally-accepted definition.

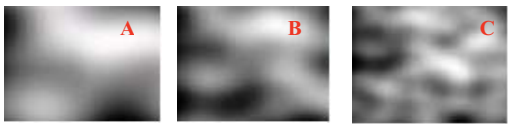

Figure 10: Musgrave's fractal textures with fixed fractal dimension of 2.5 and lacunarity parameters of A) 2, B) 3, and C) 5.

Recently, we have developed a new, more general framework for fractals that will encompass each of the three fractal features as well as rigorously define them [8–10]. Our work to date has centered on a formal definition for lacunarity [10]. This work is separate from the previous work on lacunarity [12] in that we have approached the definition through a new set of measures applied to a fractal's optimal cover. We define a cover as a set of open balls that contain all of the data under analysis, i.e., it is a set of open hyper-spheres of a given size that, when placed over the data, will contain all of it. We

define the optimal cover as the cover with the minimum number of balls, or covering elements. The simplest method to obtain such a cover in an automated process is via a clustering algorithm.

These measures are based on spanning trees formed on the optimal cover. This allows our definitions to be more general, allowing the three parameters to fully decouple into fractal dimension, lacunarity, and connectivity in a fundamental way while remaining fully connected to the topologic basis behind the fractal concept. The underlying concepts for each of these statistics might be best described through a series of simple diagrams, see Figures 11A-D.

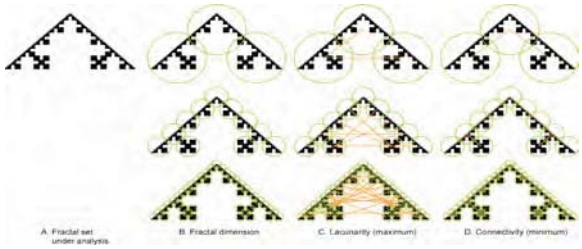

Figure 11: Above is an example of covers and spanning trees for a simple fractal data set. The covering elements are represented as green circles, while the spanning trees are shown as orange lines. Successive scales of our fractal analysis methods are demonstrated for each statistic.

Figure 11A introduces a simple fractal data set to be analyzed with each statistic. In Figure 11B, the basic concept of fractal dimension is introduced via a series of covers produced by successively smaller covering elements. One simplified measure of fractal dimension can be achieved by measuring the slope of the log-log plot of the number of covering elements versus the inverse size of the covering element along the linear portion of this curve [8–9]. Figures 11C and 11D introduce the concepts of lacunarity and connectivity [10] across successively smaller covers as being measures of the maximum and minimum spanning trees, respectively. It is through these measures on these spanning trees that we are able to investigate the lacunarity and connectivity of data across varying length scales.

In the present work, we have chosen to apply this new framework of unified fractal analysis to the copper tracer materials distributed throughout the weldments, as illustrated in Figures 4,6,7, and 9 above. The MAPPER 2.0b software program developed at the INL is used to perform this task (this is an upgraded version of the software package discussed in reference [7], which runs on Mac OS X, Linux, or Windows), see Figure 12. Using MAPPER, one can easily select a region within the large x-ray CT reconstructed data set, as shown in Figure 7, for analysis. The selection process is shown in Figure 13. Once a region for analysis has been selected, the user sets the thresholding limits, minimum and maximum grayscale values, which will allow for the conversion of the grayscale data set into a hard particle based, 3D data set, representing the trace copper material to be analyzed in our case, see figures 14 and 9.

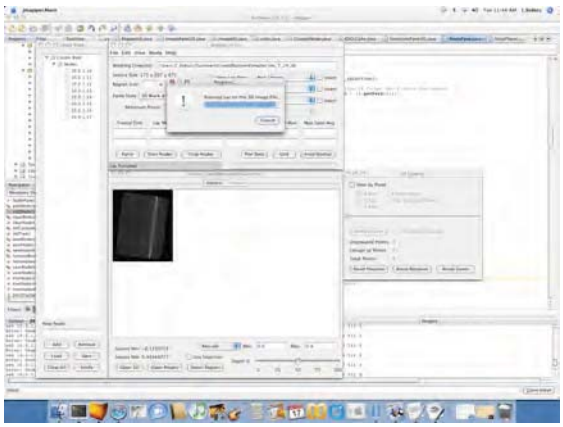

Figure 12: Mapper 2.0b, a distributed parallel processing software package currently under development at the INL for analysis of n-dimensional datasets using unified fractal statistics.

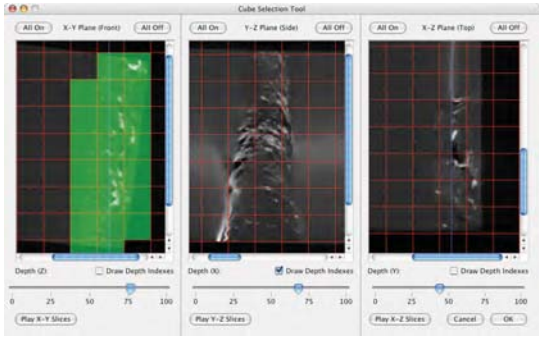

Figure 13: Mapper 2.0b, region selection process graphical user interface (GUI).

Figure 14: Mapper 2.0b, region selection process GUI.

Once the regions of interest (in this case, those containing copper) have been selected and thresholded, analysis can proceed. The results are shown as red-blue-green (RGB) translucent boxes overlaid on the data set. Numerical values can also be obtained. For the present proof-of-concept work, RGB overlays are sufficient, see Figures 15 and 16.

Figure 15: Fractal analysis of the top side of the FSW's copper tracer materials, which were isolated using the x-ray CT system for the reconstructed region shown in Figure 14.

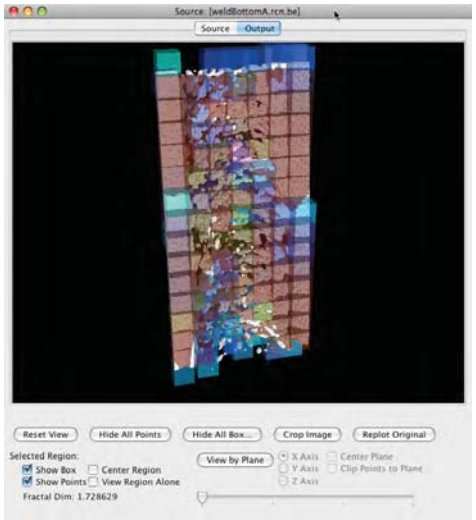

Figure 16: Fractal analysis of the bottom side of the FSW's copper tracer materials, which were isolated using the x-ray CT system for the reconstructed region shown in Figure 14.

Note that Figures 15 and 16 show a richness of RGB color for the weld under analysis. Although this weld had been assumed to be in steady state, such richness in colors implies that the structure of the copper tracer material is changing significantly along both the length and cross-section of the weld.

Conclusions

In this paper an experimental approach was used to verify the feasibility of using offline x-ray computed tomography to nondestructively analyze FSW and FSP flow patterns within the final weldments or processed material. The feasibility of this method was demonstrated in the numerically quantifiable images obtained using the unified fractal statistics approach (shown here in Figures 15 and 16), which also may be presented in animated form for further visualization. These fractal values are presented via a RGB heuristic visual overlay, which is more readily understood by the typical researcher not directly involved in fractals research –it is, in fact, more understandable to the authors as well, who are involved in fractals research. The feasibility of performing such analysis in real time, i.e. during the welding process, is beyond the focus of the paper and seems very unlikely within the near term. The unexpected richness of the RGB overlays indicates that what had been assumed to be a steady state FSW may not be, and this deserves further study. Overall, x-ray CT and fractal analysis represent two new tools that the FSW and FSP community may exploit in future research efforts to understand and better control these processes.

Acknowledgments

This work was supported through the INL Laboratory Directed Research and Development Program (LDRD) under DOE Idaho Operations Office Contract DE-AC07-05ID14517.

References

1. S. Z. Lu, D. C. Lipp, and A. Hellawell. Fractal *Analysis of Complex Microstructures in Castings, Proceedings: MC95 International Metallography Conference,* American Society for Metals, Materials Park, Ohio, pp. 119–121, 1995.
2. R. M. Summers, L. M. Pusanik, J. D. Malley and J. M. Hoeg. *Fractal analysis of virtual endoscopy reconstructions, In Medical Imaging 1999: Physiology and Function from Multidimensional Images*, Chen, C-T and Clough, AV, Eds., Proceedings of SPIE Vol. 3660, 258–269 (1999). {http://www.cc.nih.gov/drd/fractal.pdf}.
3. G. Benelli, and A. Garzelli. *Oil-spills detection in SAR images by fractal dimension estimation, IEEE Proc. IGARSS '99*, Vol. II, pp. 1123–1126.
4. Z. Lewandowski, D. Webb, M. Hamilton, and G. Harkin. *Quantifying Biofilm Structure, Wat. Sci.*

Tech., Vol. 39, Num. 7, pg. 71, 1999.
5. T. G. Smith, Jr., G. D. Lange, and W. B. Marks. *Fractal Methods and Results in Cellular Morphology -Dimensions, Lacunarity, and Multifractals, Journal of Neuroscience*, Vol. 69, pp. 123–136, 1996.
6. S. Möller, D. R. Korber, G. M. Wolffaardt, S. Molin, and D. E. Caldwell. *Impact of Nutrient Composition on a Degradative Biofilm Community, Appl. Environ. Microbiol.* Vol. 63, pp. 2432–2438.
7. S. J. Grooms, A. W. Deason, C. R. Tolle, T. R. McJunkin, and D. L. Stoner. *MAPPER: a Software Program for Quantitative Biofilm Characterization Implemented on Distributed Architecture Using Multiple Hardware and Operating System Implementations via a Secure Network Protocol, ASM,* Poster, S.L.C., UT, May 20, 2002.
8. C. R. Tolle, T. R. McJunkin, and D. Gorsich. *Sub-Optimal MCV Cover Based Method for Measuring Fractal Dimension, IEEE Tran. on Pattern Recognition and Machine Intelligence*, Vol. 25, No. 1, pp. 32-41, Jan 2003.
9. C. R. Tolle and D. Gorsich. *Sub-Optimal Covers for Measuring Fractal Dimension, Proceedings of the 1996 Rocky Mountain NASA Space Grant Consortium Conference,* Utah State University, Logan, UT, 1996.
10. C. R. Tolle, T. R. McJunkin, D. T. Rohrbaugh, and R. A. LaViolette, *Lacunarity definition for ramified data sets based on optimal cover, Physica D*, Vol. 179, No. 3-4, pp. 129–152, May 2003.
11. B. B. Mandelbrot, *The Fractal Geometry of Nature: Updated and Augmented,* W.H. Freeman and Company, New York, NY, 1983.
12. R. Plotnick, R. Gardner, W. Hargrove, K. Prestegaard, and M. Perlmutter. *Lacunarity analysis: a general technique for the analysis of spatial patterns, Physical Review E,* Vol. 53, No. 5, 5461, 1996.
13. C. R. Tolle, T. R. McJunkin and D. J. Gorsich. *An efficient implementation of the gliding box lacunarity algorithm, Physica D,* Vol. 237, No. 3, 306-315, 2008.
14. D. S. Ebert, ed. *Texturing and Modeling: A Procedural Approach*, Academic Press Professional, Cambridge, MA, 1994.
15. Barrett, H.H., and W. Swindell, *Radiological Imaging: The Theory of Image Formation, Detection, and Processing*, Academic Press, San Diego, CA, ISBN 0-12-079602-3, (1981)
16. Withers, P., *X-ray nanotomography*, *Materials Today*, Vol 12, No. 12, 26-34 (2007)
17. L.A. Feldkamp, L.C. Davis and J.W. Kress, *Practical cone-beam algorithm J. Opt. Soc. Am. A*, A6 612-19 (1984)